Magnetic Resonance Imaging 64 (2019) 71–76

Contents lists available at ScienceDirect

Magnetic Resonance Imaging

journal homepage: www.elsevier.com/locate/mri

Original contribution

Machine learning analysis of MRI-derived texture features to predict placenta accreta spectrum in patients with placenta previa

Valeria Romeo[a], Carlo Ricciardi[a], Renato Cuocolo[a,*], Arnaldo Stanzione[a], Francesco Verde[a], Laura Sarno[b], Giovanni Improta[c], Pier Paolo Mainenti[d], Maria D'Armiento[a], Arturo Brunetti[a], Simone Maurea[a]

[a] University of Naples "Federico II", Department of Advanced Biomedical Sciences, Naples, Italy
[b] University of Naples "Federico II", Department of Neuroscience, Reproductive and Dentistry Sciences, Naples, Italy
[c] University of Naples "Federico II", Department of Public Health, Naples, Italy
[d] Institute of Biostructures and Bioimaging of the National Council of Research (CNR), Naples, Italy

ARTICLE INFO

Keywords:
Placenta accrete spectrum
MRI
Texture analysis
Radiomics
Machine learning

ABSTRACT

Purpose: To evaluate whether a machine learning (ML) analysis employing MRI-derived texture analysis (TA) features could be useful in assessing the presence of placenta accreta spectrum (PAS) in patients with placenta previa (PP). The hypothesis is that TA features may reflect histological abnormalities underlying PAS in patients with PP thus helping in differentiating positive from negative cases.

Materials and methods: Pre-operative MRI examinations of 64 patients with PP of which 20 positive (12 accreta, 7 increta and 1 percreta) and 44 negative for PAS were retrospectively selected. Multiple (n = 3) rounded regions of interest (ROIs) were manually positioned on sagittal or coronal T2-weighted images over homogeneous placental tissue close to the placental-myometrial interface for each patient to extract TA features. After balancing the dataset with the Synthetic Minority Over-sampling Technique, training and testing sets were obtained using Hold-out with a 75/25% split. Different algorithms were applied on the training set using the wrapper method, which looks for the best combination of features based on the optimization of a heuristic function in order to get the highest accuracy, and a 10-fold Cross-validation. The accuracy of the best models was also assessed on the test set. Histology was used as the standard of reference.

Results: A total of 192 ROIs were positioned and a ROI-based analysis was then conducted. Among the different algorithms, *k*-nearest neighbors obtained the highest accuracy (98.1%), precision (98.7%), sensitivity (97.5%) and specificity (98.7%) while exploiting the lowest number of features (n = 26); conversely, the Naïve Bayes algorithm got the lowest scores showing an accuracy of 80.5%.

Conclusion: ML analysis using MRI-derived TA features could be a feasible tool in the identification of placental tissue abnormalities underlying PAS in patients with PP. This approach might represent an additional tool in the clinical practice, thus expanding the application field of artificial intelligence to medical images.

1. Introduction

Placental accreta spectrum (PAS) (creta, increta, percreta) is defined as trophoblasts' abnormal invasion into the myometrial layer at different invasion depth [1]. Placenta previa (PP) is a low-lying placenta completely or partially covering the internal cervical ostium. The major risk factors for PAS are represented by PP and the presence of uterine scars due to previous cesarean sections and/or uterine procedures [1]. Indeed, it is reported that the lack of re-epithelialization close to the uterine scar area may alter the placental/myometrial interface, determining cellular changes within the trophoblast. Specifically, extravillous trophoblasts appear hypertrophic and increased in numbers in PAS with reduced spiral artery remodelling [2]. Considering the possible occurrence of hemorrhage in case of placental detachment failure, the early identification of PAS is crucial for patient management [3].

In this setting, ultrasound (US) and magnetic resonance imaging (MRI) have been both reported as useful imaging techniques to identify PAS. US is the first-level imaging modality due to its large availability and lower costs. However, it suffers from high operator dependence and low reproducibility. On the other hand, MRI has the advantage of

* Corresponding author at: Department of Advanced Biomedical Sciences, University of Naples Federico II, Via S. Pansini, 5, 80123 Naples, Italy.
E-mail address: renato.cuocolo@unina.it (R. Cuocolo).

https://doi.org/10.1016/j.mri.2019.05.017
Received 30 April 2019; Received in revised form 13 May 2019; Accepted 14 May 2019

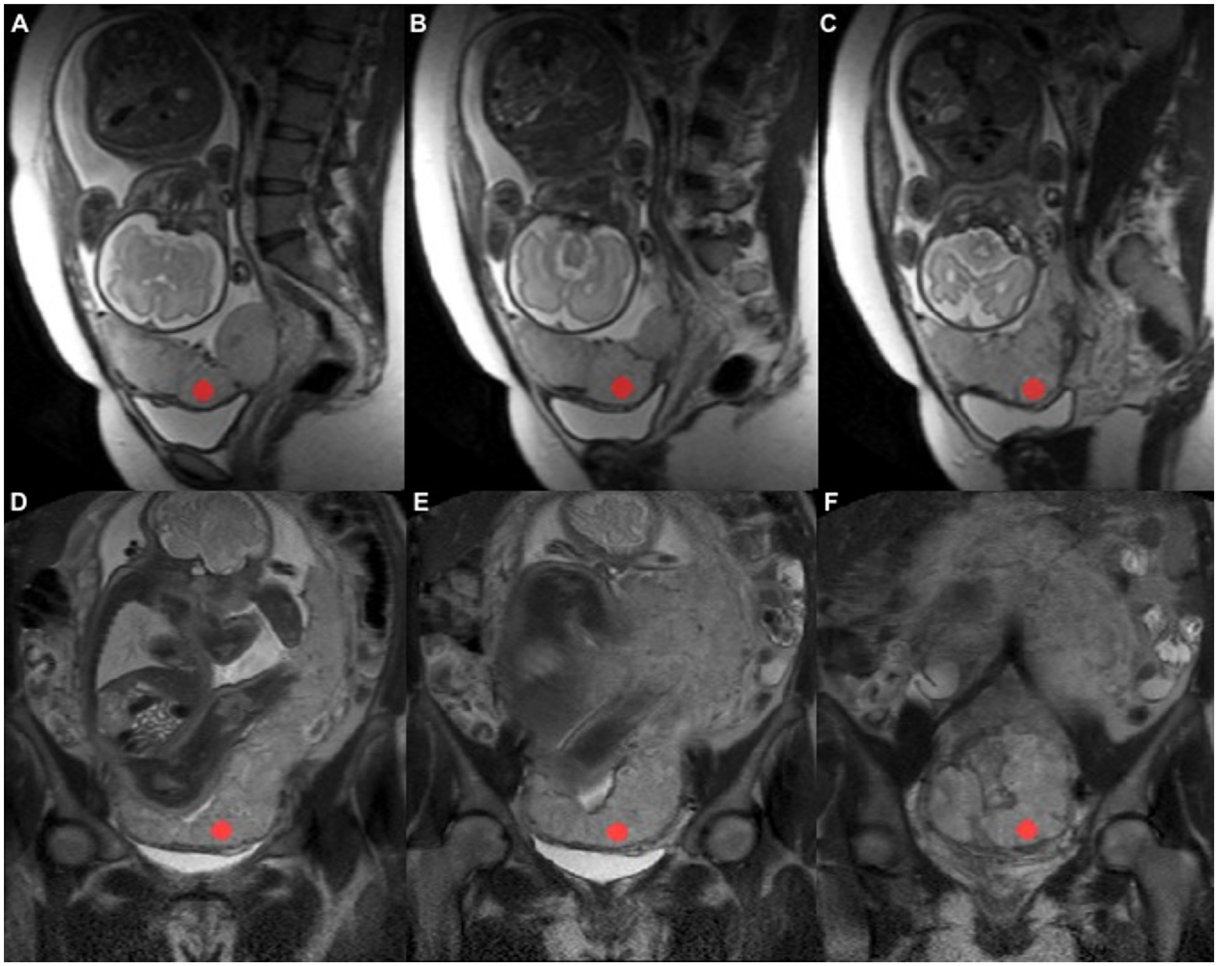

Fig. 1. Example of ROI positioning on T2-weighted images. Choice of plane i.e. sagittal (A - C) or coronal (D – F) was determined to where placental tissue was better represented allowing for ROI circles placement close to the myometrial/uterine interface on three images at a range of two slices.

providing panoramic images across different acquisition planes; furthermore, MRI image acquisition is relatively operator independent and images can be even easily subjected to later re-evaluations. Major drawbacks of MRI are related to its high costs and patient discomfort. Regarding the comparison of the diagnostic performance between the two imaging modalities in identifying PAS, variable accuracy values and conflicting results are reported [4,5], both requiring specific expertise to be correctly interpreted through the identification of specific morphological signs [6]. However, the visual qualitative analysis of images may not be completely accurate to extract the corresponding diagnostic information.

Machine learning (ML) is an application of artificial intelligence increasingly embraced in several fields of medicine such as patient outcome prediction or lesion classification. Specifically, ML can be applied to medical images through the analysis of quantitative radiomics features such as those extracted by texture analysis (TA), reflecting region of interest heterogeneity [7]. Given the wide employment of ML techniques and their promising results in both oncological and non-oncological areas [8–12] we aimed to evaluate whether ML analysis, employing MRI-derived TA features, could provide a novel methodological viewpoint useful in assessing the presence/absence of PAS in patients with PP. Our hypothesis is that TA features may reflect histological abnormalities underlying PAS in patients with PP thus helping in differentiating positive from negative cases.

2. Methods and materials

2.1. Patient population

This observational retrospective study was approved by our Institutional Review Board and written informed consent was waived. Unenhanced MRI examinations of consecutive pregnant patients with PP and US suspicion of PAS performed between January 2013 and March 2018 who underwent cesarean section (CS) in our institution were retrospectively enrolled. US criteria for suspicion of PAS consisted of the presence of US abnormal signs as recommended by FIGO consensus guidelines [13].

Inclusion criteria were: > 18-year-old patients with PP who performed an MRI examination at our institution and for whom a histological report was available. Exclusion criteria were incomplete MRI examinations due to patient claustrophobia and MRI images significantly affected by fetal/mother movements.

2.2. Pathology

All histological samples were evaluated by a pathologist expert in pediatric and perinatal analysis. On hysterectomy samples, diagnostic criteria for placenta creta and increta consisted in the attachment of chorionic villi to the myometrium with and without invasion, respectively. Placenta percreta was diagnosed when chorionic villi invaded the uterine serosa or were extended beyond it [14].

Placental samples were also analyzed to detect placental villi

alteration integrated with clinical intrapartum findings. The placenta was weighted, measured including cord and membranes, inspected in detail and systematically sectioned to identify macroscopic abnormalities; then, full thickness tissue blocks were obtained from cord, membranes and representative placental areas for subsequent formalin fixation, processing, paraffin embedding, cutting and hematoxylin/eosin staining [15].

2.3. MRI acquisition

MRI was performed using a 1.5 T scanner (Gyroscan, Intera, Philips, Best, The Netherlands) with a phased-array body coil. Turbo-spin-echo (TSE) T2-weighted sequences (FOV 405 × 321 mm, matrix: 232 × 164, slice thickness 5–6 mm, number of slice 40, Flip angle: 90°, GAP 1, TR/TE = 381/80 ms) were acquired on the three planes (axial, sagittal and coronal). Total MRI scanning duration time was approximately 15 min.

2.4. Texture analysis

2.4.1. TA features extraction

Placental location and morphology were assessed on all acquisition planes. As large datasets are preferred for machine learning classifier training, multiple (n = 3), rounded (13-pixel diameter) regions of interest (ROIs) were positioned for each patient and used for subsequent analyses. In detail, sagittal or coronal T2-weighted images were annotated over homogeneous tissue close (within 5 mm of distance from ROIs margin) to the placental-myometrial interface. Choice of plane was due to where placental tissue was better represented, allowing for correct ROI placement. If both planes were suitable, sagittal images were preferred. Details and examples of ROI positioning are illustrated in Fig. 1. A dedicated software (Pyradiomics, v2.1.2) [16] was used for the following TA feature extraction. Firstly, images underwent a normalization (scale = 100) as T2 values were not derived from quantitative T2 mapping sequences. Then, after rescaling to an isotropic 1 mm voxel, Laplacian of Gaussian, with sigma values ranging from 1 (most fine texture) to 5 (most coarse) with unitary increments, and wavelet decomposition filtering were applied.

2.4.2. Machine learning analysis

KNIME (v 3.7.1), a freely available analytics platform with possibility to integrate many other analytics software and programming languages such as Weka and R, was used in order to perform the analyses on the dataset [17]. First of all, the Synthetic Minority Oversampling Technique (SMOTE) was applied to balance the dataset [18]. It creates synthetic data points by extrapolating an object between two nearest neighbors belonging to the same class. Successively, a point along the line connecting these two objects is randomly selected, determining the new object's attributes.

The Hold-out method was used to divide the dataset in two independent parts: a training set (75% of the total sample) and a test set (the remaining 25%) [19]. Different algorithms were then applied on the training set using the Wrapper method, which looks for the best combination of features based on the optimization of a heuristic function in order to get the highest accuracy [20–23], together with a 10 fold Cross-validation. The latter splits the dataset into k folds and the model is learned k times on k-1 folds and tested on one-fold. The integration between KNIME and Weka allows employing consecutively Hold-out and the combination of Wrapper and Cross-validation. Finally, the test set was used to assess the best-performing models created with the training set. All metrics are expressed as the mean of values obtained during this cycle of validation.

2.4.3. Algorithms

Random Forest creates a large number of decision trees, based on bagging, resampling data repeatedly and training a new classifier for each sample. Each tree is trained on a diverse set of records and attributes. The row sets for each decision tree are created by bootstrapping and have the same size as the original input table. For each node of a decision tree, a new set of attributes is determined by taking a random sample of size square root of m, where m is the total number of attributes [20].

K-Nearest Neighbor (k-NN) represents one of the simplest classifiers, finding a group of k objects in the training set that are the closest to the test instance and basing the assignment of a label on the prevalence of a particular class in this neighborhood [22]. The distance from the object to be labelled to the identified k-nearest neighbors is computed, and the class labels of these nearest neighbors are then used to determine the class label of the object.

Naïve Bayes (NB) is based on the Bayes' theorem and the maximum posteriori hypothesis, assuming that the effect of an attribute on a given class is independent from the values of the other attributes (which is almost never true), it is called “conditional independence”. Classification does not require an accurate probability estimate as long as maximum probability is assigned to the correct class.

Multilayer Perceptron is an artificial neural network (ANN) which makes a local adaptation of the weight-updates consistently with the behavior of the error function. Differently from other adaptive techniques, the effect of the adaptation process is not distorted by the unpredictable influence of the size of the derivative, but only dependent on the temporal behavior of its sign. It leads to an efficient and transparent adaptation process. The algorithm follows the implementation of Riedmiller et al. [23].

3. Results

3.1. Patient population

Seventy-one consecutive unenhanced MRI scans of patients with PP and suspicion of PAS who underwent CS in our institution were retrieved. Seven patients were excluded because MRI examinations were prematurely interrupted due to claustrophobia (n = 4) or affected by fetal/mother artifact (n = 3), leaving a final population of sixty-four patients (mean age 34.4 ± 4.9 years, mean gestational age 34.6 ± 2.3 weeks). Histological samples used as standard of reference consisted of cesarean hysterectomy in all 20 cases positive for PAS (12 placenta creta, 7 placenta increta and 1 placenta percreta), according to the FIGO guidelines [24]. In cases negative for PAS clinical intrapartum findings and placental tissue were considered as standard of reference since hysterectomy was not clinically indicated. In the remaining two cases negative for PAS cesarean hysterectomy was performed due to the occurrence of hemorrhage related to uterine atony.

3.2. Texture analysis

A total of 192 ROIs were positioned, of which 165 on the sagittal plane and 27 on the coronal plane, and a ROI-based analysis was then conducted. From both the original images and filtered ones, a total of 1204 texture parameters were extracted, including: first order histogram analysis, grey level co-occurrence matrix, grey level run length matrix, grey level size zone matrix, neighboring grey tone difference matrix and grey level dependence matrix.

3.3. Dataset pre-processing

Through the balancing and amplification process, the number of ROI-based records rose to about 500, rendering the dataset balanced. Furthermore, the number of features was limited to 100, in order to reduce computation time, by applying a threshold filter to the correlation matrix of all variables; we considered correlated features with a correlation higher than 0.5. Features with high intercorrelation were also excluded as they did not add significant information to the classifier. The correlation heatmap of the extracted features is shown in

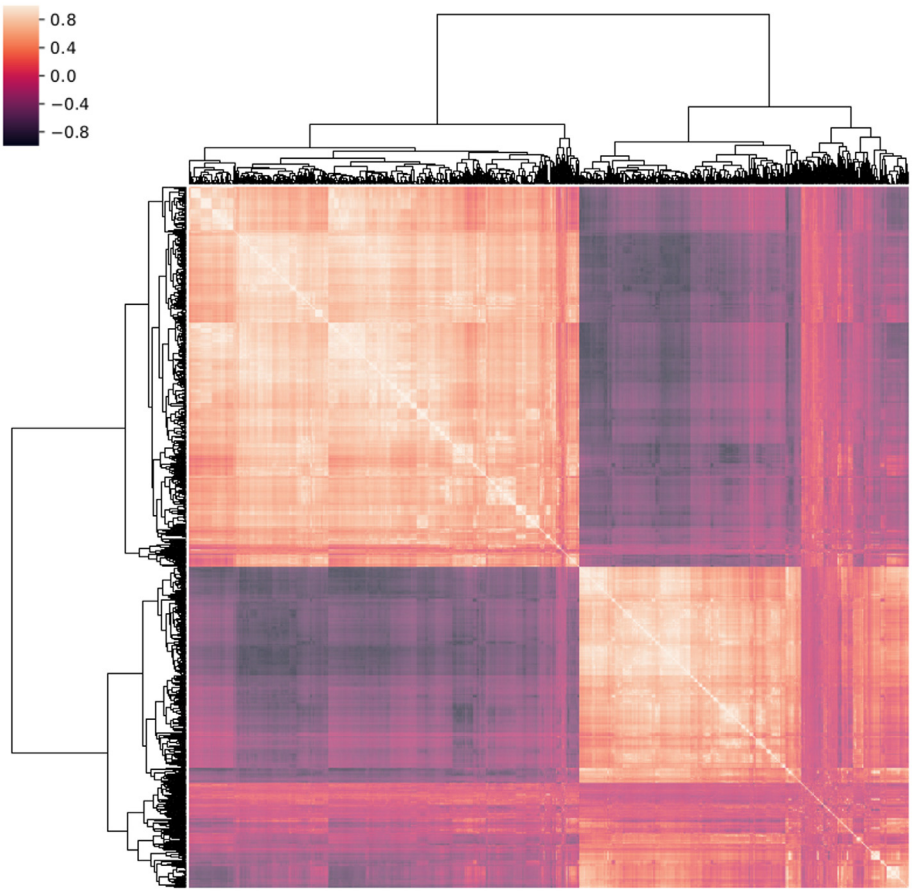

Fig. 2. Hierarchically-clustered correlation heatmap of the extracted feature matrix.

Fig. 2.

3.4. Machine learning analysis

After the creation of a model through the training set, the algorithms were applied on the independent test set, as described above; the accuracy values and relative number of attributes employed for each tested algorithm are shown in Table 1.

Among the tested algorithms, the *k*-NN obtained the highest accuracy (98.1%), precision (98.7%), sensitivity (97.5%) and specificity (98.7%) values, while exploiting the lowest number of features (26). Conversely, the Naïve Bayes algorithm got the lowest accuracy of 80.5%.

Features selected by the *k*-NN algorithm are reported in Table 2, while the workflow of all algorithms undergoing the Wrapper method is shown in Fig. 3.

Table 1
Accuracy values of the different machine learning classifiers. Values are reported as percentages.

	Accuracy	Precision	Sensitivity	Specificity	N° Features
Random forest	95.6	97.4	93.7	93.7	52
K Nearest Neighbor	98.1	98.7	97.5	98.7	26
Naïve Bayes	80.5	77.3	86.1	75.0	39
Multilayer Perceptron	88.6	84.9	92.4	83.8	40

4. Discussion

According to our experience, ML analysis employing MRI-derived TA features was useful to assess the presence of PAS in patients with PP, with an overall diagnostic accuracy of 98.1%. In detail, first, second and higher order texture features were extracted and employed by different ML classifiers using the Wrapper method. Among these, the *k*-NN algorithm obtained the highest diagnostic accuracy in diagnosing PAS employing the lowest number of features (n = 26). Conversely, the lowest diagnostic accuracy value (80.5%) was found for the NB algorithm employing a higher number of TA features (n = 39). This result was quite expected as it is a classifier with a strong assumption (the conditional independence) that was weakened by employing a large number of features. Similarly, the ANN obtained a lower diagnostic accuracy compared to the *k*-NN algorithm. This could be in part due to the relatively low number of patients, limiting the accuracy of deep learning techniques. On the other hand, it should be noted that the good accuracy shown by the *k*-NN (98.1%) in our population suggests that it could not be necessary to focus future studies on meeting the higher computational and data requirements that would be needed to potentially increase ANN accuracy in this setting.

The early detection of PAS is of crucial importance in order to establish the most appropriate surgical management and avoid the occurrence of hemorrhage during the delivery. US is the first level imaging modality to assess the presence of PAS in PP patients. A recent meta-analysis conducted on the prenatal US diagnosis of placenta creta showed that US is highly sensitive and specific when performed by expert operators [25]. Over the last years, MRI has gained relevance in this field, mainly due to an increase in its use in the clinical practice, thus leading to greater radiologist expertise. Recent studies reported high sensitivity and specificity values of MRI to detect PAS, even

Table 2
Features selected by the *k*-NN classifier that obtained the highest diagnostic accuracy of 98.1%.

log-sigma-1-0-mm-3D_glcm_Correlation	wavelet-LLH_firstorder_Median
log-sigma-2-0-mm-3D_firstorder_Kurtosis	wavelet-LLH_glcm_ClusterShade
log-sigma-2-0-mm-3D_glcm_Correlation	wavelet-LLH_glcm_Idn
log-sigma-5-0-mm-3D_firstorder_Maximum	wavelet-LLH_glrlm_RunLengthNonUniformity
log-sigma-5-0-mm-3D_glcm_Correlation	wavelet-HLH_firstorder_Median
wavelet-HLL_firstorder_Median	wavelet-HHH_firstorder_Skewness
wavelet-HLL_firstorder_Kurtosis	wavelet-HHH_firstorder_Kurtosis
wavelet-HLL_glrlm_GrayLevel NonUniformity	wavelet-HHL_firstorder_Median
wavelet-HLL_glszm_LargeAreaHighGrayLevelEmphasis	wavelet-HHL_firstorder_Kurtosis
wavelet-LHL_firstorder_Skewness	wavelet-HHL_gldm_SmallDependenceLowGrayLevelEmphasis
wavelet-LHH_firstorder_Median	wavelet-LLL_firstorder_Kurtosis
wavelet-LHH_firstorder_Mean	wavelet-LLL_gldm_LargeDependenceLowGrayLevelEmphasis
wavelet-LLH_firstorder_Skewness	original_firstorder_Skewness

suggesting new methods of image analysis through the detection of specific MRI imaging findings with an overall diagnostic accuracy of 92% [26,27], similar to that obtained by the ML classifiers in or study. However, as for US, MRI has to be performed by experienced readers in order to detect several imaging signs suggestive for PAS and achieve the best diagnostic performance. Indeed, MRI signs recognition and correct interpretation are significantly influenced by reader experience [28]. In this perspective, ML analysis using TA features extracted from MRI images represent a novel and different methodological viewpoint that could benefit less experienced radiologists in the detection of PAS or aiding experienced ones when facing doubtful cases.

A recent study assessed the feasibility of TA conducted on MRI images to depict placenta heterogeneity changes throughout gestation [29]. In detail, co-occurrence matrix features were extracted and found able to detect placental tissue heterogeneity correlated with gestational age, represented by aging of the cotyledon. Similarly, we hypothesized that TA could be useful to depict placental abnormalities underlying PAS. Particularly, modifications of extra-villous trophoblasts and blood support have been described in PAS at a microscopic level [2]. It has been also proven that such abnormalities are related to the interaction with the placenta and the decidua basalis; this is why we decided to position ROI circles close to the placenta/myometrial interface, in order to specifically depict tissue heterogeneity at that level. A similar application of TA and ML classifiers has been reported applied to US images through the extraction histogram-analysis features, founding them useful to depict placental heterogeneity in patients with gestational diabetes when using the k-nearest neighbor ML classifier [30].

The strength of the present work is represented by the application of a combined TA and ML approach to identify PAS in patients with PP; indeed, to the best of our knowledge this is the first study evaluating the possible role of artificial intelligence techniques to predict PAS using MRI images. However, our study is not free of limitations, mainly related to the relatively small sample size; this limit has been overcome by the use of a 10-fold Cross-validation, which is currently reported as a valuable methodology [11], and a Hold-out to create an independent sample of records that was used to further test the models. Furthermore, our population had an asymmetrical distribution due to the occurrence of a greater number of negative as compared to positive cases; to address this issue, artificial data have been generated to balance our dataset, which is a well-known approach to solve this issue [10,11]. Nevertheless, despite our attempts to overcome study limitations, future studies, preferably prospective and conducted on a larger cohort of patients are mandatory to confirm our results and to further assess the role of this new diagnostic approach in the clinical practice.

In conclusion, on the basis of this preliminary experience ML analysis using TA-derived features proved to be a feasible tool in the identification of PAS in patients with PP. Our findings support the hypothesis that TA and ML could aid radiologists in identifying placental tissue abnormalities underlying PAS, playing a possible role as an adjunctive tool in the clinical practice and expanding the current knowledge about further possible applications of artificial intelligence.

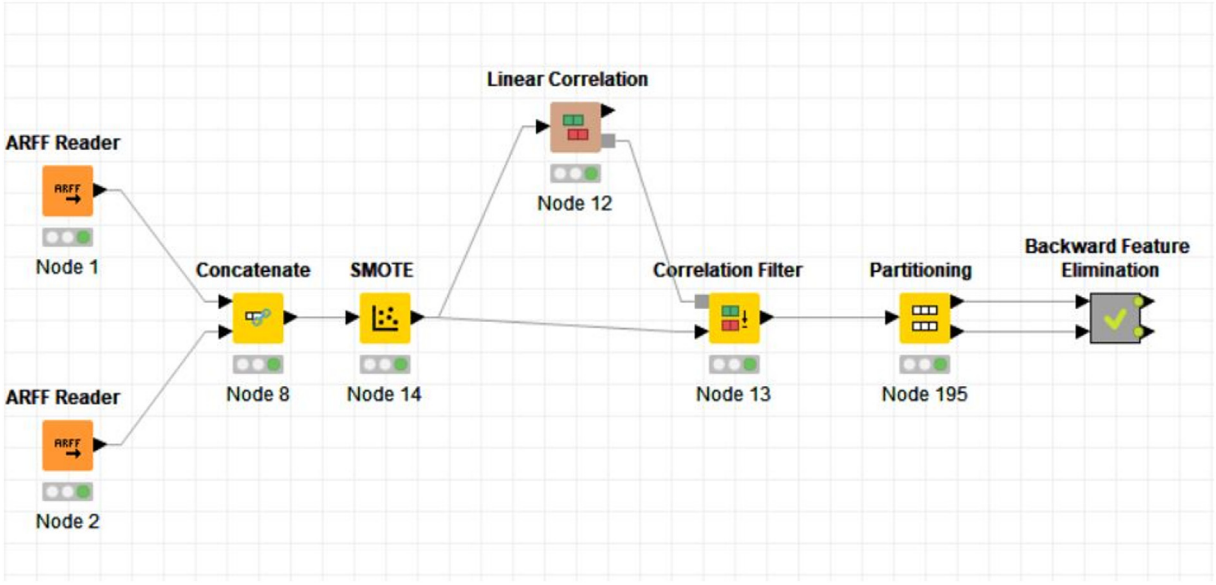

Fig. 3. Workflow describing the implementation of the Wrapper method.

Declaration of Competing Interest

The authors have no conflicts of interest to disclose.

References

[1] Fitzpatrick KE, Sellers S, Spark P, Kurinczuk JJ, Brocklehurst P, Knight M. Incidence and risk factors for placenta accreta/increta/percreta in the UK: a national case-control study. PLoS One 2012;7. https://doi.org/10.1371/journal.pone.0052893.

[2] Jauniaux E, Collins S, Burton GJ. Placenta accreta spectrum: pathophysiology and evidence-based anatomy for prenatal ultrasound imaging. Am J Obstet Gynecol 2018;218:75–87. https://doi.org/10.1016/j.ajog.2017.05.067.

[3] Esakoff TF, Sparks TN, Kaimal AJ, Kim LH, Feldstein VA, Goldstein RB, et al. Diagnosis and morbidity of placenta accreta. Ultrasound Obstet Gynecol 2011. https://doi.org/10.1002/uog.8827.

[4] Warshak CR, Eskander R, Hull AD, Scioscia AL, Mattrey RF, Benirschke K, et al. Accuracy of ultrasonography and magnetic resonance imaging in the diagnosis of placenta accreta. Obstet Gynecol 2006;108:573–81. https://doi.org/10.1097/01.AOG.0000233155.62906.6d.

[5] Einerson BD, Rodriguez CE, Kennedy AM, Woodward PJ, Donnelly MA, Silver RM. Magnetic resonance imaging is often misleading when used as an adjunct to ultrasound in the management of placenta accreta spectrum disorders. Am J Obstet Gynecol 2018;218:618.e1–7. https://doi.org/10.1016/j.ajog.2018.03.013.

[6] Elsayes KM, Trout AT, Friedkin AM, Liu PS, Bude RO, Platt JF, et al. Imaging of the placenta: a multimodality pictorial review. RadioGraphics 2009. https://doi.org/10.1148/rg.295085242.

[7] Kohli M, Prevedello LM, Filice RW, Geis JR. Implementing machine learning in radiology practice and research. Am J Roentgenol 2017;208:754–60. https://doi.org/10.2214/AJR.16.17224.

[8] Choy G, Khalilzadeh O, Michalski M, Do S, Samir AE, Pianykh OS, et al. Current applications and future impact of machine learning in radiology. Radiology 2018:171820https://doi.org/10.1148/radiol.2018171820.

[9] Erickson BJ, Korfiatis P, Akkus Z, Kline TL. Machine learning for medical imaging. RadioGraphics 2017. https://doi.org/10.1148/rg.2017160130.

[10] Romeo V, Maurea S, Cuocolo R, Petretta M, Mainenti PP, Verde F, et al. Characterization of adrenal lesions on unenhanced MRI using texture analysis: a machine-learning approach. J Magn Reson Imaging 2018;48. https://doi.org/10.1002/jmri.25954.

[11] Stanzione A, Cuocolo R, Cocozza S, Romeo V, Persico F, Fusco F, et al. Detection of extraprostatic extension of cancer on biparametric MRI combining texture analysis and machine learning: preliminary results. Acad Radiol 2019:1–7. https://doi.org/10.1016/j.acra.2018.12.025.

[12] Nie D, Zhang H, Adeli E, Liu L, Shen D. 3D deep learning for multi-modal imaging-guided survival time prediction of brain tumor patients. Lect Notes Comput Sci (Includ Subser Lect Notes Artif Intell Lect Notes Bioinformatics) 2016. https://doi.org/10.1007/978-3-319-46723-8_25.

[13] Jauniaux E, Bhide A, Kennedy A, Woodward P, Hubinont C, Collins S, et al. FIGO consensus guidelines on placenta accreta spectrum disorders: prenatal diagnosis and screening. Int J Gynecol Obstet 2018. https://doi.org/10.1002/ijgo.12408.

[14] Oyelese Y, Smulian JC. Placenta previa, placenta accreta, and vasa previa. Obstet Gynecol 2006. https://doi.org/10.1097/01.AOG.0000207559.15715.98.

[15] Bartels HC, Postle JD, Downey P, Brennan DJ. Placenta accreta spectrum: a review of pathology, molecular biology, and biomarkers. Dis Markers 2018. https://doi.org/10.1155/2018/1507674.

[16] Van Griethuysen JJM, Fedorov A, Parmar C, Hosny A, Aucoin N, Narayan V, et al. Computational radiomics system to decode the radiographic phenotype. Cancer Res 2017. https://doi.org/10.1158/0008-5472.CAN-17-0339.

[17] Warr WA. Scientific workflow systems: pipeline pilot and KNIME. J Comput Aided Mol Des 2012;26:801–4. https://doi.org/10.1007/s10822-012-9577-7.

[18] Chawla NV, Bowyer KW, Hall LO, Kegelmeyer WP. SMOTE: synthetic minority over-sampling technique. J Artif Intell Res 2002. https://doi.org/10.1613/jair.953.

[19] Kohavi R, Sommerfield D. Feature subset selection using the wrapper method: overfitting and dynamic search space topology. First Int Conf Knowl Discov Data Min. 1995.

[20] Breiman L. Random Forrest. Mach Learn 2001. https://doi.org/10.1023/A:1010933404324.

[21] Friedman JH. Greedy function approximation: a gradient boosting machine. Ann Stat 2001. https://doi.org/10.1214/aos/1013203451.

[22] Wu X, Kumar V, Quintan JR, Ghosh J, Yang Q, Moloda H, et al. Top 10 algorithms in data mining. Knowl Inf Syst 2008. https://doi.org/10.1007/s10115-007-0114-2.

[23] Riedmiller M, Braun H. A direct adaptive method for faster backpropagation learning: the RPROP algorithm. IEEE Int Conf Neural Networks-Conf Proc 1993. https://doi.org/10.1109/ICNN.1993.298623.

[24] Allen L, Jauniaux E, Hobson S, Papillon-Smith J, Belfort MA, Duncombe G, et al. FIGO consensus guidelines on placenta accreta spectrum disorders: nonconservative surgical management. Int J Gynecol Obstet 2018. https://doi.org/10.1002/ijgo.12409.

[25] Jauniaux E, Bhide A. Prenatal ultrasound diagnosis and outcome of placenta previa accreta after cesarean delivery: a systematic review and meta-analysis. Am J Obstet Gynecol 2017;217:27–36. https://doi.org/10.1016/j.ajog.2017.02.050.

[26] Maurea S, Romeo V, Mainenti PP, Ginocchio MI, Frauenfelder G, Verde F, et al. Diagnostic accuracy of magnetic resonance imaging in assessing placental adhesion disorder in patients with placenta previa: correlation with histological findings. Eur J Radiol 2018;106:77–84. https://doi.org/10.1016/j.ejrad.2018.07.014.

[27] Valentini AL, Gui B, Ninivaggi V, Miccò M, Giuliani M, Russo L, et al. The morbidly adherent placenta: when and what association of signs can improve MRI diagnosis? Our experience. Diagn Interv Radiol 2017;23:180–6. https://doi.org/10.5152/dir.2017.16275.

[28] Alamo L, Anaye A, Rey J, Denys A, Bongartz G, Terraz S, et al. Detection of suspected placental invasion by MRI: Do the results depend on observer' experience? Eur J Radiol 2013;82:e51–7. https://doi.org/10.1016/j.ejrad.2012.08.022.

[29] Do QN, Lewis MA, Madhuranthakam AJ, Xi Y, Bailey AA, Lenkinski RE, et al. Texture analysis of magnetic resonance images of the human placenta throughout gestation: a feasibility study. PLoS One 2019: 1–11. doi:https://doi.org/10.1371/journal.pone.0211060.

[30] Malathi G, Shanthi DV. Histogram based classification of ultrasound images of placenta. Int J Comput Appl 2010;1:58–61. https://doi.org/10.5120/343-522.